NJC

ROYAL SOCIETY OF CHEMISTRY

PAPER

View Article Online
View Journal

Cite this: DOI: 10.1039/d6nj00545d

Thermal and (photo-)catalytic properties of poly(*N*-isopropylacrylamide)-stabilised gold nanoparticles induced by radiolysis

Tawakalit D. Abdulyekeen, [a] Cécile Sicard-Roselli, [a] Vincent Huc, [b] Hynd Remita [a] and Isabelle Lampre *[a]

Gold nanoparticles (AuNPs) are widely studied due to their unique physicochemical properties, which are highly dependent on their size, shape, and composition. Efficient and environmentally friendly synthesis methods and effective stabilisation agents are essential for fabricating AuNPs with controlled sizes and shapes. This study explores the radiolytic synthesis method, a green synthesis approach using ionising radiation (gamma irradiation), and investigates the use of a thermosensitive polymer, poly(*N*-isopropylacrylamide) (PNIPAM), and its monomer, *N*-isopropylacrylamide (NIPAM), for stabilising gold nanoparticles in aqueous solutions. The resulting PNIPAM-AuNPs and NIPAM-AuNPs were spherical, homogenously dispersed, with average sizes of 5.4 nm and 3.5 nm, respectively, and exhibited high stability at room temperature over a long time. Thermal analysis revealed enhanced thermal responsiveness for PNIPAM-AuNPs, an effect not observed with the NIPAM-AuNPs. The AuNPs demonstrated excellent catalytic activity in the reduction of 4-nitrophenol (4-NP) in the presence of sodium borohydride and showed efficient plasmonic photocatalytic activity in the visible-light-driven reduction of 4-nitrothiophenol (4-NTP). These findings support the potential of radiolytically synthesised polymer-stabilised AuNPs for catalysis and environmental remediation applications.

Received 11th February 2026,
Accepted 14th April 2026

DOI: 10.1039/d6nj00545d

rsc.li/njc

Introduction

Gold nanoparticles have attracted significant attention due to their unique properties, which are largely influenced by their size, shape, and environment.[1,2] For instance, they present interesting optical properties which arise from localised surface plasmon resonance (LSPR). LSPR refers to the collective oscillation of electrons confined in the conduction band on the surface of the nanoparticles, resulting in absorption bands in the visible domain.[3–5] These optical characteristics have enabled their use in a wide range of applications, including sensing,[6,7] imaging,[8] energy conversion[9] and biomedicine.[10] Gold nanoparticles also exhibit remarkable catalytic activity, due to their distinct electronic, chemical and structural properties when compared to bulk gold metal.[11] The versatility of gold nanoparticles can be attributed to their large surface-to-volume ratio, high energy, electron confinement and the electric fields surrounding them.[12–14]

One of the major challenges associated with synthesising metallic nanoparticles (MNPs) in solution is stabilising them against aggregation for a long period of time.[15] This instability arises from their inherently high surface energy (excess energy associated with surface atoms), resulting from their high surface-to-volume ratio.[15] This surface energy makes it difficult to control the morphology of MNPs, as they tend to aggregate easily due to attractive forces such as van der Waals forces, especially in the absence of counteracting forces. These attractive effects can be mitigated using a stabilising agent that can provide steric and/or electrostatic stability to the MNPs, allowing control over their size and shape and preserving their properties. These stabilisers include polymers,[15–17] ligands,[18] surfactants,[19] and supports.[20] They are chosen based on the morphology and specific applications desired for the MNPs. Polymer-based stabilisation is one of the most effective strategies for preventing nanoparticle aggregation over extended periods. This approach enhances the stability of nanoparticles and facilitates the formation of hybrid materials with unique physical and chemical properties.[16] This dual functionality not only preserves the intrinsic characteristics of the nanoparticles but also introduces additional functionality by combining the intrinsic properties of both components, thereby broadening their range of potential applications.[15,16,21] Various types of polymer networks have been employed for nanoparticle stabilisation, including latex particles,[22] polyelectrolyte brushes,[23] stimuli-responsive polymers, *etc.*[24–27]

[a] *Université Paris-Saclay, CNRS, Institut de Chimie Physique UMR 8000, 91400 Orsay, France. E-mail: isabelle.lampre@universite-paris-saclay.fr*
[b] *Université Paris-Saclay, CNRS, Institut de Chimie Moléculaire et des Matériaux, UMR 8182, 91400 Orsay, France*

Thermosensitive polymers are a class of stimuli-responsive polymers that exhibit changes in response to environmental modifications, in this case, temperature. The use of these temperature-responsive polymers has led to the development of novel materials whose physicochemical properties can be easily tuned for potential applications such as catalysis, medicine, smart material devices, *etc.*[15,27,28] Usually, thermosensitive polymers exhibit a miscibility change in aqueous solutions in response to temperature: if dissolution is caused by heat, there is an upper critical solution temperature (UCST), while if a phase separation occurs by heating, a lower critical solution temperature (LCST) exists.[29] These thermosensitive polymers, which can be either synthetic or natural, include poly(*N*-isopropyl acrylamide) (PNIPAM),[30] poly(*N*-diethyl acrylamide) (PDEAm),[31] poly[oligo (ethylene glycol) methacrylate] (POEGMA),[32] *etc.* Poly(*N*-isopropylacrylamide) (PNIPAM) is a thermally responsive polymer that undergoes a reversible phase transition with a change in temperature in aqueous medium.[25,33,34] This transition involves a conformational change in the PNIPAM chain, ranging from a disordered state and random coil to an ordered, collapsed globule state.[35] Above its lower critical solution temperature (LCST) of about 32 °C, the PNIPAM polymer becomes hydrophobic and undergoes chain collapse, which leads to aggregation in solution due to hydrophobic interactions and hydrogen bonding fluctuation.[27] In contrast, the polymer is hydrophilic and appears soluble below its LCST due to the hydrophilic group on the polymer chain undergoing strong hydrogen bonds with the surrounding water molecules.

PNIPAM has been one of the most widely used smart polymers in the stabilisation/coating of metallic nanoparticles (gold, silver, *etc.*), resulting in a core–shell system with the nanoparticles embedded in the polymer shell.[16,17,26,36] The use of thermosensitive polymer (PNIPAM) for stabilising metallic nanoparticles enables the design of a nanomaterial composite with enhanced properties, combining the thermal switching properties of the polymer with the surface plasmon effect of the metallic nanoparticles for potential applications.[27,37,38] These nanocomposite materials have been achieved utilising several methods, such as the mixing of pre-formed thiol-terminated PNIPAM and AuNPs,[26] *in situ* chemical reduction of gold salts in the presence of PNIPAM,[27,37] *in situ* polymerisation of NIPAM and reduction of gold salt,[39] or the growth of polymer chains on the surface of the AuNPs.[16,40]

Several studies have reported the stabilisation of AuNPs with PNIPAM, investigated their thermal properties and explored their use in catalysis. Du *et al.*[27] synthesised noble metal nanoparticles (Au, Pt, Pd) stabilised by PNIPAM *via* liquid-phase reduction using ascorbic acid and sodium borohydride as reducing agents. The formed MNPs demonstrated efficient catalytic activity in the reduction of nitroarenes. Among them, PNIPAM-AuNPs stood out due to their excellent stability and high catalytic performance. Zhu *et al.*[39] employed gamma radiation to prepare thermosensitive PNIPAM-AuNP composite hydrogels through *in situ* monomer polymerisation and simultaneous reduction of gold salts using a high irradiation dose (>70 kGy). The obtained composites also exhibited efficient catalytic activity. In efforts to study the thermosensitive properties of PNIPAM-AuNPs, Jones *et al.*[16] and Li *et al.*[26] examined the effect of free PNIPAM chains in the colloidal solutions on the conformational changes of PNIPAM anchored to the AuNP surface upon heating. Jones *et al.*[16] suggested that hydrophobic interactions between free polymer chains and those on the nanoparticles' surface promoted aggregation upon temperature increase. In contrast, Li *et al.*[26] argued that the observed turbidity was due to free PNIPAM alone, and not conformational changes in surface-bound PNIPAM. However, differences in the nanoparticle synthesis methods and end groups of PNIPAM used in these studies make direct comparisons difficult.

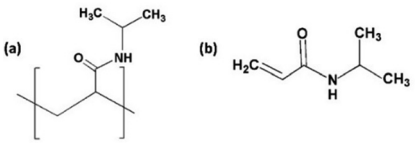

Fig. 1 Chemical structure of (a) PNIPAM and (b) NIPAM.

In order to better understand the thermoresponsive behaviour of PNIPAM and NIPAM-stabilised gold nanoparticles and to investigate their plasmonic activities, we present here the radiolytic synthesis of AuNPs stabilised by either PNIPAM or NIPAM monomers (Fig. 1). Indeed, radiolytic synthesis has emerged as a powerful technique for effectively controlling the size and shape of metallic nanoparticles in solutions or in heterogeneous media. This method involves the irradiation of the sample solutions containing metallic ions and stabilising agents by ionising radiation.[41–44] Hence, the nanoparticles are formed *via* the reduction of the Au^{III} ions in aqueous solution in the presence of PNIPAM or NIPAM, using gamma radiation. In this paper, we investigate the thermal behaviour and study the catalytic and photocatalytic ability of the formed PNIPAM-AuNPs and NIPAM-AuNPs using model reactions easily followed spectroscopically: the reduction of hexacyanoferrate(III) ($[Fe(CN)_6]^{3-}$),[45,46] and the reduction of 4-nitrophenol (4-NP) and 4-nitrothiophenol (4-NTP) used as model pollutants.[47] Taking advantage of the thermosensitivity of the polymer, the present study aims to establish the role played by plasmonic heating and hot-electron generation upon plasmon excitation of the gold nanoparticles.

Experimental section

Materials

Gold(III) chloride trihydrate ($HAuCl_4.3H_2O$, ≥99.9%), *N*-isopropylacrylamide (NIPAM, ≥99%), poly(*N*-isopropylacrylamide) (PNIPAM, M_n-40 000, 100%), sodium hydroxide (NaOH, ≥98%), *tert*-butanol ($(CH_3)_3COH$, ≥99.7%), 4-aminophenol (4-AP, C_6H_7NO, 98%), 4-nitrothiophenol (4-NTP, $C_6H_5NO_2S$, 80%), 4-nitrophenol (4-NP, $C_6H_5NO_3$, ≥99.5%), sodium borohydride ($NaBH_4$, 98%), 2-propanol (99.5%), potassium hexacyanoferrate(III) ($K_3[Fe(CN)_6]$), and triethanolamine (TEOA, $C_6H_{15}NO_3$, ≥99%) were all purchased from Sigma-Aldrich, and used without any further purification. All the aqueous solutions were prepared with ultrapure water (Millipore system, 18.2 MΩ cm).

All glassware were washed with aqua regia and thoroughly washed with deionised water before use.

Synthesis of PNIPAM-AuNPs and NIPAM-AuNPs

PNIPAM- or NIPAM-stabilised AuNPs were synthesised using the radiolytic method. Stock aqueous solutions of 0.2 M PNIPAM or NIPAM, and 25 mM $HAuCl_4$, were initially prepared. To a vial containing 18.79 mL of water, 785 μL of the PNIPAM or NIPAM solution and 118 μL of the metallic salt solution were added, making the final concentrations 7.84×10^{-3} M for PNIPAM or NIPAM and 1.48×10^{-4} M for the Au atoms. The solution mixture was sonicated for 10 minutes to ensure homogeneity, and then vigorously stirred for 30 minutes at room temperature. 310 μL of propan-2-ol (0.2 M) was added to the mixture as a scavenger for oxidising species generated during irradiation. The solutions were then deaerated by bubbling nitrogen gas through them for 30 minutes to remove dissolved oxygen, and were kept under a N_2 atmosphere during the subsequent irradiation. The sample solutions were irradiated by gamma radiation with different doses to achieve complete reduction, using a ^{60}Co panoramic source with a dose rate of 1.8 kGy h^{-1}.

Catalytic tests

The reduction of hexacyanoferrate(III) ($[Fe(CN)_6]^{3-}$) in the presence of triethanolamine (TEOA), and the reduction of 4-nitrophenol (4-NP) and 4-nitrothiophenol (4-NTP) by sodium borohydride ($NaBH_4$) were conducted to study the catalytic activity of the synthesised PNIPAM-AuNPs and NIPAM-AuNPs. The reactions were carried out in alkaline solutions at room temperature. The UV-visible absorption spectra were monitored at different time intervals to investigate the catalytic efficiency.

Alkaline aqueous solutions of PNIPAM-AuNP or NIPAM-AuNP catalysts ($[Au^0]$ = 0.148 mM, pH around 11) were obtained by adding a few drops of 0.15 M NaOH aqueous solution. Aqueous solutions containing 2 mM $[Fe(CN)_6]^{3-}$, or 0.489 mM 4-NP, or 0.163 mM 4-NTP were prepared, and the pH of the solutions was adjusted in the range of 10–11 before use by adding a small amount of a 0.15 M NaOH aqueous solution.

In the case of 4-NP and 4-NTP, this adjustment resulted in a colour change of the solutions, from pale yellow to dark yellow (Fig. S1, inset) and changes in the UV-visible absorption spectra (Fig. S1). These changes are due to the formation of phenolate ions resulting from deprotonation of the phenolic group[27] (pK_a = 7.15 for 4-NP[48] and 4.71 for 4-NTP[49]). The protonated form of 4-NP (4-NTP) absorbs at 317 nm (305 nm), while the phenolate ion presents a maximum absorption at 400 nm (405 nm) (Fig. S1). 0.5 mL of the alkaline 4-NP solution was then added to a reactor containing 2.49 mL of water ([4-NP] = 0.0815 mM). Then, 1.25 mg of $NaBH_4$ was added to the mixture ($[NaBH_4]$ = 11 mM) to achieve a concentration of the reducing species 135 times greater than the initial concentration of 4-NP; subsequently, 10.9 μL of the catalyst solution was then added to the sample mixture ($[Au^0]$ = 0.538 μM). The solution was kept in the dark by covering the cuvette with aluminium foil due to the sensitivity of the catalysts and pollutants to light; then, UV-visible absorption spectra were recorded at 10-minute intervals. In the case of 4-NTP, 1.5 mL of the 4-NTP solution, 1.5 mL of water, 1.5 mg of $NaBH_4$ and 10.9 μL of the catalyst solution were used to ensure similar concentrations of catalysts and pollutants as in the case of 4-NP, *i.e.*, the reaction mixture contained 0.0815 mM 4-NTP, 11 mM $NaBH_4$, and 0.538 μM catalyst.

For the reduction of $[Fe(CN)_6]^{3-}$, 750 μL of a $K_3Fe(CN)_6$ stock solution was added to a reactor, followed by 2.2 mL of the catalyst solution and 60 μL of TEOA. The solution containing 0.5 mM $K_3Fe(CN)_6$, 0.02 M TEOA, and 0.1077 mM catalyst (Au^0) was then deaerated by bubbling nitrogen gas for 10 minutes and kept in the dark by wrapping the cuvette with aluminium foil. UV-visible absorption spectra were also recorded at 10-minute intervals.

Photocatalytic tests

The photocatalytic activity of the synthesised AuNPs was evaluated by using the catalysts in the reduction of 4-nitrophenol (4-NP), 4-nitrothiophenol (4-NTP), and hexacyanoferrate(III) ($[Fe(CN)_6]^{3-}$). As for the catalytic tests, alkaline solutions of PNIPAM-AuNP or NIPAM-AuNP catalysts ($[Au^0]$ = 0.148 mM, pH around 11) were prepared, as well as stock solutions of 4-NP (0.489 mM), 4-NTP (0.163 mM), and $Fe(CN)_6^{3-}$ (2 mM).

For the nitroarene reduction, the reaction mixtures containing 4.35×10^{-5} M of either 4-NP or 4-NTP and 1.077×10^{-4} M of either PNIPAM-AuNPs or NIPAM-AuNPs were added to a 1 cm optical pathlength quartz cuvette sealed with a septum cap. The solutions were deaerated by bubbling nitrogen gas through them for 40 minutes to remove dissolved oxygen and to allow maximum adsorption of pollutant molecules on the surface of the NPs (Fig. S14). The solutions were then illuminated using a solar lamp (Solar Simulator LS0306, 300 W Xe light) positioned 16 cm from the sample to ensure uniform illumination or a homemade LED reactor (525 nm) (Fig. S2). A 500 nm long-pass colour filter (Fig. S2a) was used with the solar lamp to prevent the direct photoactivation of 4-NTP while exciting the AuNPs LSPR around 520 nm. The photocatalytic reaction was then monitored by recording the UV-visible absorption spectra at 1-hour intervals.

For the photocatalytic reduction of $[Fe(CN)_6]^{3-}$, solutions containing 5×10^{-4} M of $K_3Fe(CN)_6$ and 1.11×10^{-4} M of catalyst (Au^0) were prepared. The solutions were deaerated by bubbling nitrogen gas for 10 minutes, and then illuminated using the LED reactor as described above.

Characterisation

UV-visible absorption spectra were recorded using either a single HP8543 UV-vis spectrophotometer or a double-beam UV-1900i UV-vis spectrophotometer equipped with a temperature controller. Transmission electron microscopy (TEM) was performed using a JEOL JEM-1400 electron microscope operating at an accelerating voltage of 120 kV. Prior to analysis, a small volume of the nanoparticle sample was sonicated to ensure dispersion and homogeneity. An aliquot of the sonicated sample was taken and deposited onto a TEM grid using the drop-casting method.[50] The TEM grids used were 200-mesh

copper grids, coated with carbon or Formvar to support the nanoparticles. The samples were allowed to dry at room temperature before imaging with a CCD camera. The micrographs were then analysed using ImageJ software. Dynamic light scattering (DLS) measurements were performed using a Malvern ZetaSizer ZEN3600. Acquisitions were performed with a nanoparticle concentration of 0.148 mM with a 173° backscattered angle. ^{1}H NMR spectra were recorded in D_2O using a 400 MHz Bruker TopSpin spectrometer.

Results and discussion

Radiolytic synthesis and thermal properties of the stabilised AuNPs

Stabilisation by PNIPAM. The UV-visible absorption spectra of the aqueous solutions containing 1.48×10^{-4} M $HAuCl_4$, 7.84×10^{-3} M PNIPAM, and 0.2 M propan-2-ol before and after irradiation at different doses are shown in Fig. 2a. Before irradiation, the spectrum presents an absorption band around 300 nm due to the $Au^{III}Cl_4^-$ ions. After irradiation, this band has vanished, and an absorption band with a maximum at 528 nm is observed for all irradiation doses. This absorption band is characteristic of the LSPR of AuNPs. No significant difference in the spectra is noticed with increasing the dose from 0.7 kGy to 1.1 kGy. This indicates that at an irradiation dose of 0.7 kGy, all the $Au^{III}Cl_4^-$ ions present in the aqueous solution are reduced. It should be noted that the spectra of irradiated aqueous solutions containing only PNIPAM do not show any absorption in the visible range (Fig. 2a), indicating that the observed absorption band arises solely from the AuNPs. The narrow LSPR band observed for the synthesised PNIPAM-AuNPs, with a maximum absorbance at 528 nm, suggests the formation of small spherical nanoparticles.

The stability of the PNIPAM-AuNPs synthesised at an irradiation dose of 1.1 kGy was investigated. The nanoparticles remained stable over several days, as evidenced by the absence of significant changes in the spectra recorded a few days after synthesis (Fig. S3). Furthermore, the solution remained stable for several months, indicating effective stabilisation by PNIPAM. A similar result has already been reported by Du *et al.*, who mentioned that the chemically synthesised PNIPAM-AuNPs remained stable for a long time (over six months).[27]

The TEM micrographs of the PNIPAM-AuNPs synthesised with an irradiation dose of 1.1 kGy and their particle size distribution are shown in Fig. 2b and c. The obtained nanoparticles have a spherical shape and appear polydisperse. The average diameter of the PNIPAM-AuNP gold core is estimated to be 5.4 ± 1.8 nm (Fig. 2c), which is consistent with the absorption spectra (Fig. 2a).

Stabilisation by NIPAM. The UV-visible absorption spectra of the aqueous solutions containing 1.48×10^{-4} M $HAuCl_4$, 7.84×10^{-3} M NIPAM, and 0.2 M propan-2-ol before and after irradiation at different doses are shown in Fig. 2d. As in the case of PNIPAM, the initial band at 300 nm due to $Au^{III}Cl_4^-$ disappears upon irradiation, and the characteristic LSPR band of AuNPs is observed at around 520 nm. The absorption spectra of the NIPAM-AuNPs did not show significant differences with a dose increase from 0.7 kGy to 1.1 kGy: only a mild increase in the absorbance was observed at the 1.1 kGy irradiation dose. These observations indicate the total reduction of the $Au^{III}Cl_4^-$ ions, as in the case of PNIPAM. Additionally, the spectrum of the irradiated solution containing only NIPAM showed no absorption band in the visible range (Fig. 2d).

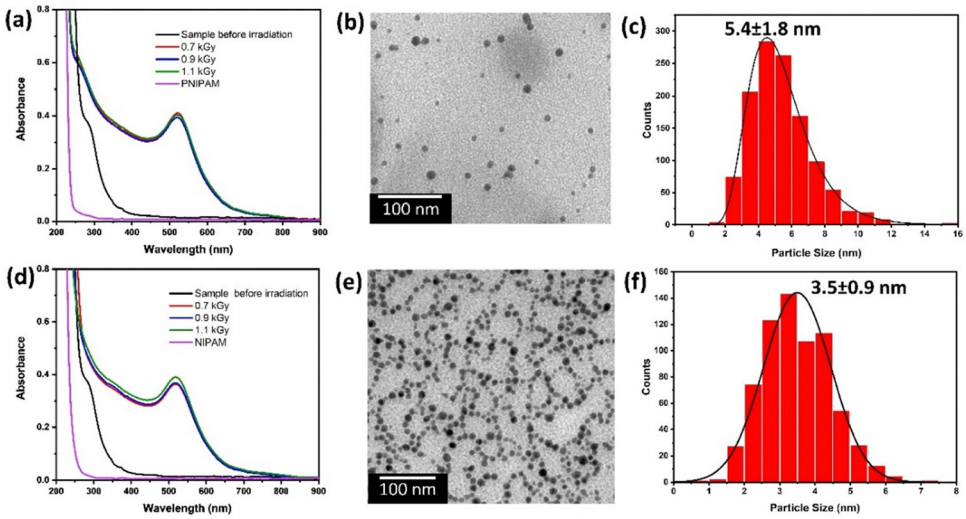

Fig. 2 (a) Absorption spectra of aqueous solutions containing 1.48×10^{-4} M $HAuCl_4$, 7.84×10^{-3} M PNIPAM, and 0.2 M propan-2-ol before and after irradiation at different doses, and absorption spectrum of an irradiated aqueous solution containing only PNIPAM (dose: 1.1 kGy). (b) TEM micrograph and (c) the diameter size distribution of the synthesised PNIPAM-AuNPs (irradiation dose: 1.1 kGy), AuNPs counted: 1204. (d) Absorption spectra of aqueous solutions containing 1.48×10^{-4} M $HAuCl_4$, 7.84×10^{-3} M NIPAM, and 0.2 M propan-2-ol before and after irradiation at different doses, and absorption spectrum of an irradiated aqueous solution containing NIPAM (dose: 1.1 kGy). (e) TEM micrograph and (f) the diameter size distribution of the synthesised NIPAM-AuNPs (irradiation dose: 1.1 kGy, AuNPs counted: 689).

The TEM micrographs of the NIPAM-AuNPs synthesised with an irradiation dose of 1.1 kGy, and their particle size distribution are shown in Fig. 2e and f. The obtained nanoparticles are spherical and appear monodisperse, with an average size of 3.5 ± 0.9 nm, slightly smaller than that of PNIPAM-AuNPs (Fig. 2f). They also present a necklace-like organisation (Fig. 2e).

As for PNIPAM, the NIPAM-AuNPs are stable in solution as the absorption spectrum of the solution recorded a day after the irradiation is identical to that shown in Fig. 2d. Nevertheless, in contrast to the PNIPAM-AuNPs, these spectra were not recorded immediately after irradiation. Indeed, a change in colour of the NIPAM-AuNP solution is observed immediately after irradiation: the initially purple-coloured solution turns pink after a couple of hours (Fig. 3a, inset). The spectrum registered immediately after irradiation differs from the others as it presents a broader absorption band. To study this phenomenon, several parameters were varied, including the concentration of the metallic salt, the concentration NIPAM, and the use of *tert*-butanol as a scavenger instead of propan-2-ol. However, similar results were observed in all cases. The narrowing of the absorption band, coupled with the colour change, indicates an evolution in the particle size and distribution, which is confirmed by TEM images. Immediately after synthesis, the nanoparticles appear elongated (Fig. 3b), while a couple of hours after synthesis, the NIPAM-AuNPs were spherical, monodisperse, and free from aggregation (Fig. 2e).

Thermal heating of PNIPAM-AuNPs and NIPAM-AuNPs. The thermoresponsive properties of the synthesised PNIPAM- and NIPAM-stabilised AuNPs were investigated using dynamic light scattering (DLS) measurements and temperature-controlled UV-visible spectroscopy at temperatures below and above the lower critical solution temperature (LCST) of PNIPAM.

Fig. 4 presents the hydrodynamic sizes of the PNIPAM-AuNPs, NIPAM-AuNPs, irradiated and non-irradiated PNIPAM measured in aqueous solution using dynamic light scattering at temperatures ranging from 25 °C to 45 °C. In the absence of irradiation, the phase transition temperature (PTT) of PNIPAM is found to be 33 °C, a typical value for pure PNIPAM, and the apparent hydrodynamic diameter changes from ~25 nm below the LCST up to 220 nm above it. After irradiation, the PTT of PNIPAM is lowered, ~30 °C, and the apparent diameters below and above the PTT are increased, 180 nm and 400 nm, respectively. These results indicate changes in the polymer structures due to reactions with the radiolytic species. This suggests that irradiation induces crosslinking within the PNIPAM chains, which restricts chain mobility and facilitates an earlier coil-to-globule transition upon heating. The smaller size observed in the non-irradiated PNIPAM (Fig. 4) can also be attributed to the absence of crosslinking, allowing polymer chains to remain more dispersed in solution.

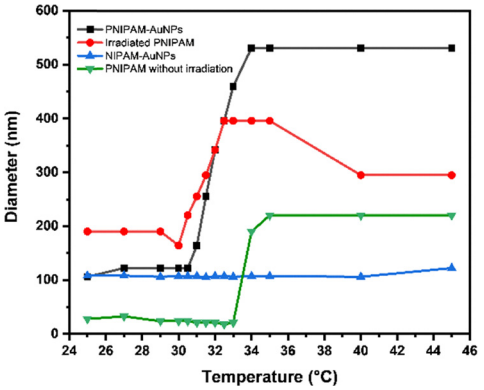

Fig. 4 Hydrodynamic sizes measured by dynamic light scattering for PNIPAM-AuNPs, NIPAM-AuNPs, irradiated PNIPAM, and non-irradiated PNIPAM at different temperatures.

For PNIPAM-AuNPs (Fig. 4), the PTT is observed to be slightly higher (~30.5 °C) than that of the irradiated PNIPAM-only solution (~30 °C). Below this PTT, no significant change in nanoparticle size is observed. However, above the PTT, a marked increase in the hydrodynamic size of PNIPAM-AuNPs is observed, reaching a plateau at around 34 °C. At elevated temperature, DLS measurements show a narrow size distribution with a single peak around 531 nm (Fig. S4), indicating the formation of a larger polymeric matrix with embedded AuNPs. The absence of additional peaks (Fig. S4) supports the idea that the nanoparticles are not freely dispersed but incorporated into the collapsed polymer network due to hydrophobic interactions of PNIPAM above the LCST. This thermal response confirms the thermosensitive behaviour of the PNIPAM layer.

The larger hydrodynamic sizes observed by DLS, compared to those measured *via* TEM, are expected due to the swollen state of the hydrated polymer layer in aqueous solutions below the LCST.[15] The irradiated PNIPAM-only solution showed slightly larger hydrodynamic sizes below the PTT than the PNIPAM-AuNPs. This difference can be attributed to the absence of competition for reducing species produced during irradiation, which allows more polymer network formation, resulting in larger sizes in DLS measurements. However, above the PTT, the sizes of the irradiated PNIPAM-only solution were smaller than those of the PNIPAM-AuNPs. This is consistent with the formation of polymer aggregates in aqueous solution, where the PNIPAM collapses into compact structures, while in PNIPAM-AuNPs, the presence of embedded AuNPs leads to larger average particle sizes. It is worth noting that the decrease

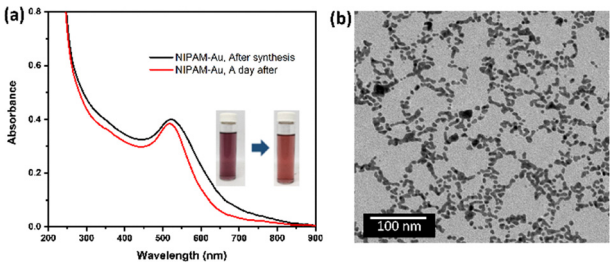

Fig. 3 (a) Absorption spectra of the irradiated aqueous solution (dose: 1.1 kGy) taken on different days (optical path length: 1 cm) (inset: images of the NIPAM-AuNP solution after synthesis and a day after). (b) TEM micrograph images of the NIPAM-AuNPs deposited immediately (after synthesis).

in size observed for the irradiated PNIPAM-only solution at temperatures of 40 °C and 45 °C can be attributed to the increased expulsion of water and enhanced collapse of the PNIPAM chains as the temperature rises. This leads to more compact structures due to stronger hydrophobic interactions.

In contrast, the hydrodynamic size of PNIPAM-AuNPs remains relatively constant from 34 °C and above, suggesting that the embedded AuNPs hindered additional polymer chain collapse. In contrast to PNIPAM-AuNPs, the hydrodynamic size of the NIPAM-AuNPs remains unchanged whatever the temperature (Fig. 4). This indicates the absence of the thermoresponsive behaviour typically associated with PNIPAM. However, the larger hydrodynamic sizes determined by DLS, compared to those measured by TEM, suggest the presence of oligomeric layers adsorbed onto the surface of the AuNPs.

Fig. 5 shows the UV-vis extinction spectra of the PNIPAM-AuNPs and NIPAM-AuNPs at 25 °C (below PTT), 40 °C (above PTT), and after cooling back down to 25 °C. PNIPAM-AuNPs showed noticeable broadening and deformation of the extinction spectrum at elevated temperature (Fig. 5a). This may be attributed to significant light scattering related to the formation of large polymer aggregates due to polymer hydrophobic interactions above the LCST, as evidenced from DLS measurements. It is important to note that no purification by centrifugation was performed prior to analysis, so possible free crosslinked PNIPAM chains remaining in the colloidal solution may favour such aggregation.[16] Upon cooling back down to 25 °C, PNIPAM rehydrates and swells, recovering its original conformation and restoring the original SPR absorption spectra (Fig. 5a). This rules out the possibility of AuNP aggregation upon heating, as the strong interactions between the outer PNIPAM layer and water molecules stabilise the nanoparticles, thereby preventing irreversible aggregation.[51,52] These spectral changes confirm the reversible thermoresponsive behaviour of the PNIPAM-AuNPs and strongly indicate the presence of a functional PNIPAM layer around the AuNPs. In contrast, for the NIPAM-AuNPs at 40 °C, no significant band broadening or deformation in the extinction spectrum is observed (Fig. 5b). The LSPR band of the NIPAM-AuNPs exhibits a minor red shift upon heating, but some light scattering is present. This suggests the formation of more compact, dense structures around the AuNPs, inducing changes in the local dielectric environment and slightly larger particles, as measured by DLS, but without polymer chain collapsing. The absence of pronounced thermoresponsive behaviour or spectra deformation supports the hypothesis that only monomers or short-chain NIPAM oligomers are present on the AuNPs surface. Upon cooling back down to 25 °C, the original spectrum is recovered, with a slight red shift observed, which remains constant after repeated heating and cooling cycles, suggesting a change in the local dielectric environment induced by heating.

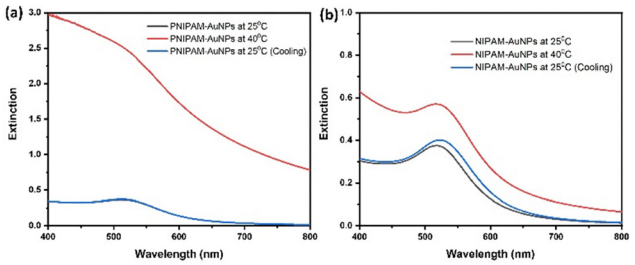

Fig. 5 Temperature-controlled UV-visible extinction spectrum obtained for PNIPAM-AuNPs (a) and NIPAM-AuNPs (b) at temperatures below and above the LCST.

Plasmonic heating. The effect of plasmonic heating due to the AuNPs stabilised by PNIPAM or NIPAM was also studied by irradiating the synthesised PNIPAM-AuNP and NIPAM-AuNP samples with the same set-up as those used for photocatalysis, *i.e.*, the LED reactor and the solar lamp.[53]

Fig. S5 presents the UV-visible absorption spectra obtained before and after one hour of light-irradiation of the colloidal solutions of PNIPAM-AuNPs and NIPAM-AuNPs under the solar lamp and LED reactor. Prior to illumination, both colloidal solutions appear clear, and their absorption spectra present the characteristic LSPR band of AuNPs. After one hour of illumination under the solar lamp, the NIPAM-AuNP solution remains visually unchanged (Fig. S5b, inset), and a slight red shift is observed in the LSPR absorption band (Fig. S5b). In contrast, after one hour of irradiation, the PNIPAM-AuNP colloidal solution becomes visibly cloudy (Fig. S5a, inset), and the corresponding UV-vis absorption spectrum shows a very broad band with a non-well-defined maximum around 550 nm (Fig. S5). This spectrum resembles that registered at 40 °C (Fig. 5a) and could indicate an increase in temperature. Indeed, after 1 h of illumination under the solar lamp, the measured temperature is approximately 46 °C. This temperature is significantly higher than that measured after one hour of solar lamp illumination for non-irradiated and irradiated PNIPAM solutions (around 32.6 °C and 32 °C, respectively, close to the LCST). Indeed, even in the absence of AuNPs, a thermosensitive response is observed, as evidenced by changes in the absorption spectra (Fig. S6). This result indicates that the illumination by the solar lamp induces a rise in the temperature of the entire solution, which is increased by the presence of the AuNPs.[54] Therefore, we deduce that the observed thermosensitive behaviour in the PNIPAM-AuNPs sample (Fig. S5a) is likely due to a combined effect of both an overall heating due to the lamp and a plasmonic heating from the AuNPs.

To further investigate the role of plasmonic heating, experiments were conducted using a 525 nm LED reactor. After one hour of illumination under the LED reactor (Fig. S5), the PNIPAM-AuNP and NIPAM-AuNP colloidal solutions remain visually unchanged, and no broadening or shift in the LSPR absorption was observed (Fig. S5c and d). The temperature changes were around 5 °C, slightly higher than the measured change for the PNIPAM solutions (~4 °C). Since this temperature is below the LCST of PNIPAM, neither turbidity in the PNIPAM-AuNP solution nor spectral changes were observed. These results show that the general heating is mainly due to the absorption of the infrared photons emitted by the solar lamp since it is not observed with the LED reactor emitting only at 525 nm. However, they also suggest that, once the LCST is

reached, the collapsed state of the polymer around the nanoparticles favours the diffusion of the heat due to the plasmonic excitation.[55] Indeed, it was reported that for a gold NP surface coated by a polymer layer, the thermal resistance decreases as the polymer density increases, and that the heat transfer is favoured for a polymer with good terminal interactions with water to lower the contact resistance.[56] Here, the final temperature (around 46 °C) obtained under solar lamp illumination for the PNIPAM-AuNP solutions is higher than that reached by the PNIPAM solutions (around 32 °C, the LCST). So, the observed temperature rise might be attributed to plasmonic heating from the gold nanoparticles upon light absorption, which contributes to the overall warming of the colloidal solution.[54,57]

Discussion on the synthesis. The primary effects of the gamma radiation on a diluted aqueous solution containing metallic ions and stabilisers are the excitation and ionisation of the solvent molecules. This step is followed by dissociation, solvation, ion–molecule reactions, and dimerization, leading to the generation of highly reactive primary species, such as radicals ($H^{\bullet}$, $^{\bullet}OH$), and solvated electrons (e^-_{aq}), as well as less reactive molecular species (H_2, H_2O_2).[41,42,58] At neutral pH, the radiolytic yields, G, of these species (*i.e.* the quantity of species formed per Joule of deposited energy) are (in μmol J^{-1}): $G(e^-_{aq}) = 0.28$, $G(H^{\bullet}) = 0.06$, $G(^{\bullet}OH) = 0.28$, $G(H_2) = 0.04$ and $G(H_2O_2) = 0.07$.[59]

The radiolytic reduction of $Au^{III}Cl_4^-$ ions and the formation of AuNPs in aqueous solutions have already been studied in detail.[43,60] The Au^{III} ions in the solution are reduced to Au atoms by the strong reducing agents produced during radiolysis, the hydrogen atom ($^{\bullet}H$), and solvated electrons (e^-_{aq}) with redox potentials of $E^{\circ}(H^+/H^{\bullet}) = -2.3\ V_{SHE}$ and $E^{\circ}(H_2O/e^-_{aq}) = -2.87\ V_{SHE}$ respectively.[41,42] However, strong oxidising species, $^{\bullet}OH$ radicals with a redox potential of $E^{\circ}(^{\bullet}OH/H_2O) = +2.76\ V_{SHE}$,[41] are also generated and may oxidise Au atoms and ions to higher oxidation states. To prevent this, secondary or tertiary alcohols (propan-2-ol or *tert*-butanol in this study) are used to scavenge the oxidising species. The resulting propan-2-ol radicals may further participate in metallic ion reduction ($E^{\circ}(CH_3)_2CO/(CH_3)_2C^{\bullet}OH) = -1.8\ V_{SHE}$ (eqn (1)–(5)).[41,42]

$$Au^{III}Cl_4^- + e^-_{aq} \rightarrow Au^{II}Cl_4^{2-} \quad (1)$$

$$2Au^{II}Cl_4^{2-} \rightarrow Au^{III}Cl_4^- + Au^{I}Cl_2^- + 2Cl^- \quad (2)$$

$$(CH_3)_2CHOH + {}^{\bullet}OH\ (H^{\bullet}) \rightarrow (CH_3)_2C^{\bullet}OH + H_2O\ (H_2) \quad (3)$$

$$Au^{I}Cl_2^- + e^-_{aq} \rightarrow Au^{0}Cl_2^{2-} \quad (4)$$

$$Au^{I}Cl_2^- + (CH_3)_2C^{\bullet}OH \rightarrow Au^{0}Cl_2^{2-} + (CH_3)_2CO + H^+ \quad (5)$$

In our study, at an irradiation dose of 0.7 kGy, all the $Au^{III}Cl_4^-$ ions present in the aqueous solution ($[Au^{III}Cl_4^-] = 1.48 \times 10^{-4}$ M) are reduced, which corresponds to a reduction yield G_{red} of 0.63×10^{-6} mol J^{-1}. This was estimated using the formula:

$$D = \frac{zC}{\rho G}$$

where D is the dose (in Gy), z is the charge of the metallic ion, C is the ion concentration (in mol L^{-1}), ρ is the solution density (1 kg L^{-1}), and G is the radiolytic yield (in mol J^{-1}). This indicates that both the solvated electron and the reducing alcohol radicals are involved in the reduction process ($G(e^-_{aq}) + G(H^{\bullet}) + G(^{\bullet}OH) = 6.2 \times 10^{-7}$ mol J^{-1}). The reduction process goes with nucleation to form stable nanoparticles (Fig. 6).

However, in the presence of PNIPAM or NIPAM, the generated radiolytic species may also react with PNIPAM and NIPAM molecules, and so, radicals and radical anions are generated from the PNIPAM or NIPAM through additions to the unsaturated or double bonds in these compounds (eqn (6) and (7)).[58,61,62]

$$NIPAM + e^-_{aq} \rightarrow (NIPAM)^{\bullet -} \quad (6)$$

$$NIPAM + H^{\bullet} \rightarrow (H\text{–}NIPAM)^{\bullet} \quad (7)$$

During the reduction process involving NIPAM, a competition may arise between metallic ions and NIPAM for reducing species, particularly solvated electrons, due to their high reactivity with NIPAM. Using literature rate constants ($k_6 = 1.0 \times 10^{10}\ M^{-1}\ s^{-1}$ for NIPAM and $k_1 = 5.7 \times 10^9\ M^{-1}\ s^{-1}$ for Au^{III}),[58,63] and the concentrations used in this study, the estimated rates of electron scavenging are $7.84 \times 10^7\ s^{-1}$ for NIPAM and $8.44 \times 10^5\ s^{-1}$ Au^{III} ions, indicating that NIPAM reacts preferentially with solvated electrons. Nevertheless, the high redox potential reported for Au^{III} and Au^{II} ($E^{\circ}(Au^{III}/Au^{II}) \approx +0.7\ V_{NHE}$, $E^{\circ}(Au^{II}/Au^{I}) \approx +0.9\ V_{NHE}$)[60] compared to the estimated redox potential reported for NIPAM ($E^{\circ}(NIPAM/NIPAM^{\bullet -}) \approx -0.45$ V),[58] could lead to the metallic ions being reduced by the radical anion of NIPAM on

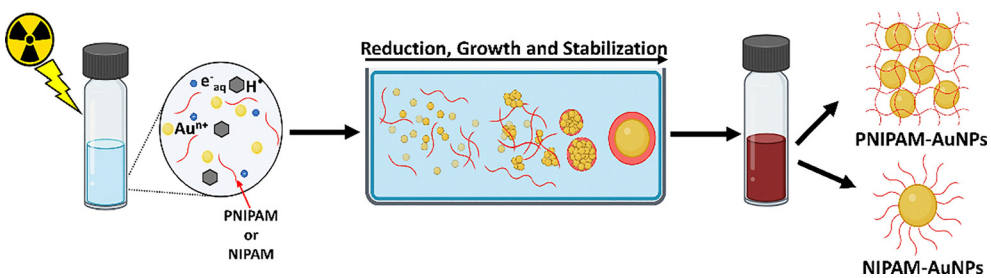

Fig. 6 Schematic illustration of the reactive species generated by the radiolysis of an aqueous solution and reduction process (created in https://BioRender.com).

the formed metal clusters. Subsequently, the Au^0 formed can reduce NIPAM ($E^\circ(Au^I/Au^0) \approx -1.5\ V_{NHE}$).[64] However, it should be noted that the redox potentials of Au^{III}, Au^{II}, and Au^I depend on their complexation state and increase with the nucleation n of the clusters (Au_n),[65] so several electron transfers may occur between gold and NIPAM, affecting the multistep reduction processes and the formation of AuNPs.

Depending on the concentration, the generated PNIPAM or NIPAM radicals can propagate to form either crosslinked hydrogels or linear polymers. In the case of PNIPAM, crosslinking is evidenced by the significant size increase observed both below and above the LCST *via* DLS in irradiated PNIPAM solution compared to non-irradiated PNIPAM solution (Fig. 4).[66] The crosslinking also induces a slight decrease in the LCST. In the case of NIPAM, the large hydrodynamic diameter determined by DLS measurements, compared to the AuNP size obtained by TEM, suggests the presence of oligomers, which effectively stabilise the AuNPs by adsorption onto their surface through complexation between nitrogen atoms and the metal ions (Fig. 6). It is assumed that no polymer formation occurred during the reduction process, as the characteristic thermosensitive behaviour associated with PNIPAM is absent upon heating the NIPAM-AuNP colloidal solution (Fig. S5b, inset). However, further characterisation using ^1H NMR spectroscopy has revealed the absence of peaks corresponding to the NIPAM monomer (Fig. S7 and S8), but the presence of broad peaks around 1.6 and 2.2 ppm in the NIPAM-AuNPs spectrum (Fig. S7). These peaks resemble those recorded for PNIPAM with a slight shift, indicating that polymerisation occurred during gamma irradiation. Due to the lack of thermosensitive behaviour, it is likely that only short-chain polymers or oligomers are formed. This may result from the competition reactions between the metallic ions and NIPAM with the radiolytic species, as well as multiple electron-transfer events between them, as previously discussed. Nevertheless, these oligomers are sufficient to efficiently stabilise the formed AuNPs, since the NIPAM-AuNP solutions are stable over several months, as are the PNIPAM-AuNP solutions.

Catalytic and photocatalytic properties of PNIPAM-AuNPs and NIPAM-AuNPs

The catalytic and photocatalytic properties of the synthesised AuNPs have been investigated using two model reduction reactions.

Reduction of hexacyanoferrate, $[Fe(CN)_6]^{3-}$. The catalytic and photocatalytic activities of the AuNPs were investigated by monitoring the reduction of $[Fe(CN)_6]^{3-}$ under different conditions: (i) in the presence of AuNP nanoparticles and triethanolamine (TEOA) (sacrificial electron donor) in the dark and under 525 nm illumination, (ii) with TEOA only, and (iii) with AuNPs only.

Fig. 7a and b show the temporal evolution of the UV-visible absorption spectra of a solution containing $K_3Fe(CN)_6$, NIPAM-AuNPs, and TEOA in the dark and under LED illumination. In both cases, a gradual decrease in the absorption band at 420 nm, characteristic of $[Fe(CN)_6]^{3-}$, is observed at 10-minute intervals, with complete reduction achieved after 2 hours. The LSPR band of the AuNPs remains quite unchanged throughout the process, confirming their stability. TEOA being in excess, the reduction reactions are shown to follow first-order kinetics with a similar rate constant (Fig. S9), indicating no effect of light on the reaction rate, contrary to previous reports.[57,67] To rule out

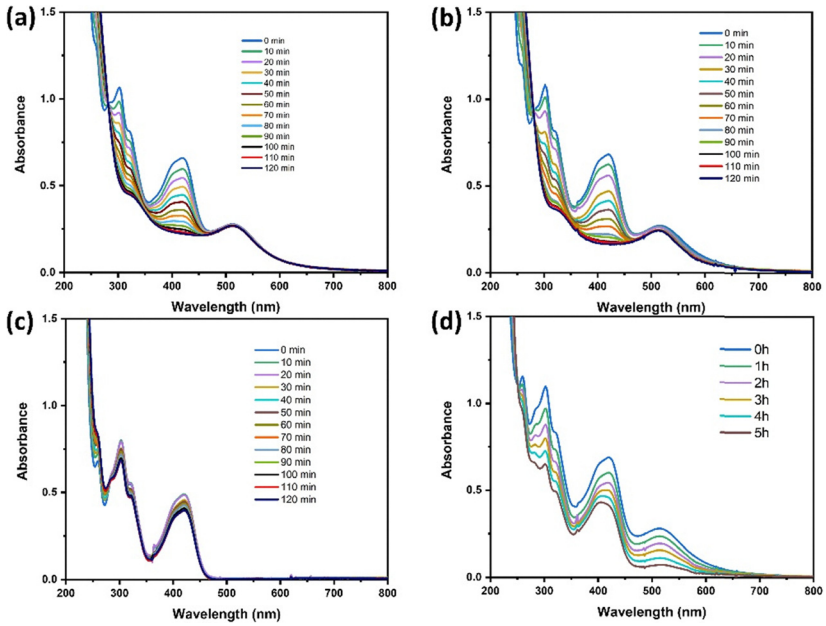

Fig. 7 Temporal evolution of the absorption spectra of aqueous solutions containing: (a) and (b) 5×10^{-4} M $K_3Fe(CN)_6$, 0.02 M TEOA and 1.077×10^{-4} M NIPAM-AuNPs (a) in the dark; (b) under LED illumination (λ = 525 nm); (c) 5×10^{-4} M $K_3(CN)_6$ and 0.02 M TEOA without NIPAM-AuNPs under LED illumination and; (d) 5×10^{-4} M $K_3Fe(CN)_6$ and NIPAM-AuNPs ($[Au^0] = 1.11 \times 10^{-4}$ M) without TEOA under LED illumination.

direct reduction of $[Fe(CN)_6]^{3-}$ by TEOA, a control experiment containing $[Fe(CN)_6]^{3-}$ and TEOA in the absence of AuNPs under LED illumination was performed (Fig. 7c). Only a very slow decrease in the $[Fe(CN)_6]^{3-}$ band is observed. In the absence of TEOA (Fig. 7d), both the $[Fe(CN)_6]^{3-}$ band at 420 nm and the AuNPs LSPR band decrease upon illumination, whereas no significant decrease is observed in the dark (Fig. S10). This indicates that the reduction of $[Fe(CN)_6]^{3-}$ is concomitant with AuNP degradation under light illumination. Similar results were also observed for PNIPAM-AuNPs (Fig. S11).

Reduction of nitrophenol (4-NP) and nitrothiophenol (4-NTP). The catalytic activity of PNIPAM-AuNPs and NIPAM-AuNPs for the reduction of 4-NP by $NaBH_4$ is presented in Fig. 8. With both catalysts, the initial yellow solution becomes transparent after less than two hours (Fig. 8a and b, inset). In the recorded absorption spectra of the solutions, the initial absorption peak of 4-NP (at 400 nm) gradually decreases, while two new peaks at 300 nm and 236 nm appear (Fig. 8a and b). These peaks correspond to 4-aminophenol (4-AP), a less toxic compound compared to 4-NP, which is used in the production of drugs.[68] This attribution is based on the recorded UV-visible spectrum of a solution containing commercial 4-AP at the expected final concentration, showing the peaks at 300 nm and 236 nm, with the same intensities (Fig. S12). The decrease in absorbance of 4-NP at 400 nm over time is shown in Fig. 8c. Complete reduction of 4-NP is achieved in 100 minutes with PNIPAM-AuNPs and 50 minutes with NIPAM-AuNPs. The difference in catalytic activity may be attributed to two effects: the size difference of the AuNPs and the accessibility of the active sites.[69] In both cases, an induction time of around 20 minutes is observed. As $NaBH_4$ is in excess compared to 4-NP (factor 135), the decays of 4-NP may be considered to follow pseudo-first-order kinetics, and the apparent rate constants (k_{app}) are found to be 0.109 min^{-1} for NIPAM-AuNPs and 0.0405 min^{-1} for PNIPAM-AuNPs (Fig. 8c, inset). The reduction of 4-NP by $NaBH_4$ in the absence of catalysts was also attempted. As shown in Fig. S13, the recorded spectra present no decrease in the absorbance after 100 minutes, indicating that no reaction occurs. This confirms that the presence of either PNIPAM-AuNPs or NIPAM-AuNPs is essential for catalytic activity, highlighting their effectiveness as catalysts for the reduction of 4-NP. The catalytic activity of the AuNPs was also studied for the reduction of 4-NTP, but no reaction was observed within 60 minutes.

The plasmonic photocatalytic activity of PNIPAM and NIPAM-stabilised AuNPs for the reduction of 4-NTP in the absence of $NaBH_4$ and under solar lamp illumination is represented in Fig. 9. Time 0 corresponds to the start of the illumination after 40 min of N_2 bubbling in the dark, allowing adsorption of 4-NTP onto the surface of the AuNPs. The effective adsorption of 4-NTP onto the AuNP surface is indicated by the difference between the UV-visible spectrum recorded for the mixture and the one calculated by the sum of the spectra of the two compounds (Fig. S14). When the mixed solution is placed under visible light irradiation, the absorption peak of 4-NTP at 409 nm gradually decreases. This decrease is accompanied by the appearance of a weak absorption band at around 270 nm and, in the case of NIPAM-AuNPs, an isosbestic point at around 344 nm, which may correspond to the formation of 4-ATP. After 7 hours of light irradiation, roughly two-thirds of the 4-NTP have disappeared in the presence of NIPAM-AuNPs, and one-half with PNIPAM-AuNPs. A complete degradation of 4-NTP was observed after keeping the sample solution for one day without covering it with aluminium foil (Fig. 9). Throughout the reaction process, the LSPR bands at 530 nm and 534 nm for the NIPAM-AuNPs and PNIPAM-AuNPs, respectively, remain stable (Fig. 9a and b). However, it has to be noted that, while the solution of NIPAM-AuNPs with 4-NTP remains clear under visible light illumination, the solution of PNIPAM-AuNPs becomes turbid due to overall heating of the solution and thermal response of the polymer, as mentioned previously. So, the spectra shown in Fig. 9a were recorded a few minutes after illumination, after the solution had cooled down and become clear again. That may explain irregularities and the absence of an isosbestic point in the case of PNIPAM-AuNPs. Fig. 9c gives the temporal evolution of the absorbance at 409 nm due to 4-NTP (after subtraction of the NPs' absorbance). The absorbance decays appear quasi-linear with time, suggesting that the reaction follows pseudo-zero-order kinetics with similar rate constants. The degradation

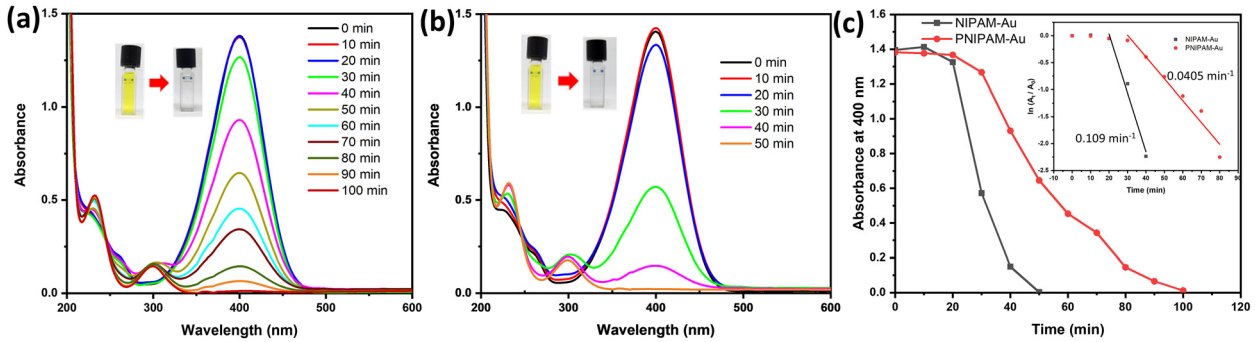

Fig. 8 Temporal evolution of the absorption spectra of an aqueous solution containing initially 0.0815 mM 4-NP, 11 mM $NaBH_4$, and (a) PNIPAM-AuNPs and (b) NIPAM-AuNPs as a catalyst ($[Au^0]$ = 0.538 μM) at various time points. (c) Plots of the absorbance at 400 nm *versus* time (inset, plots of ln (A_t/A_0) as a function of time).

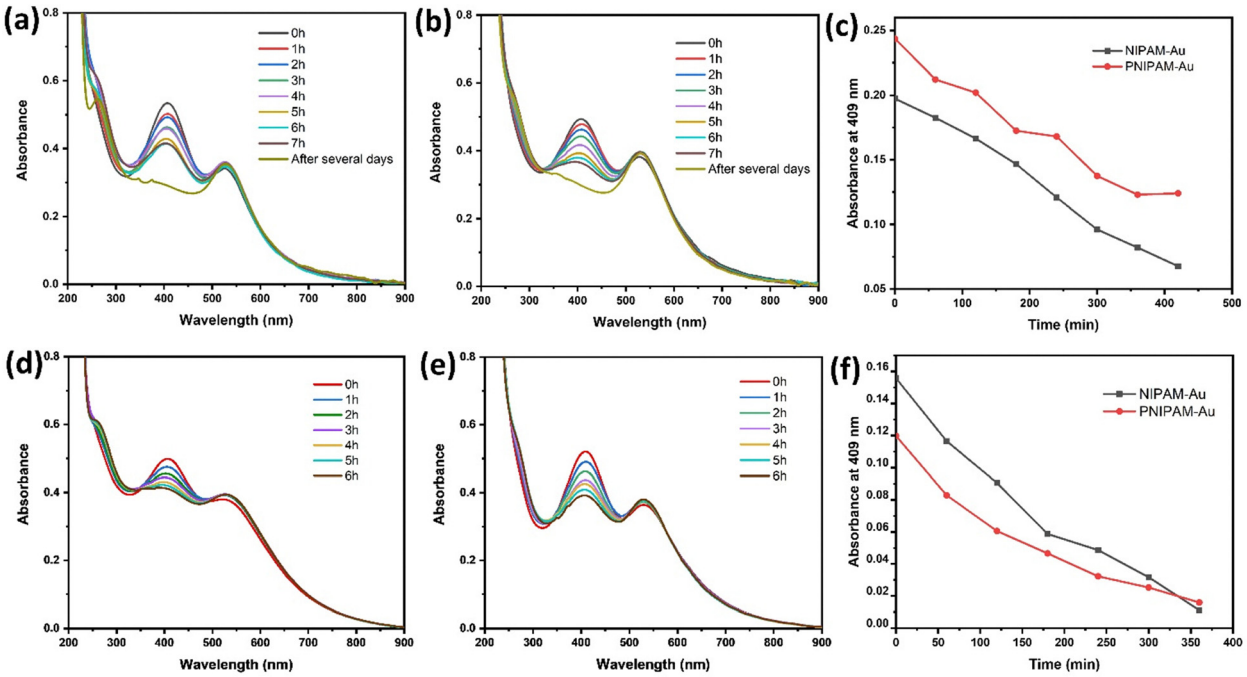

Fig. 9 Temporal evolution of the absorption spectra of aqueous solution containing initially 4.35×10^{-5} M 4-NTP with (a) PNIPAM-AuNPs and (b) NIPAM-AuNPs ($[Au^0] = 1.077 \times 10^{-4}$ M) under solar lamp illumination for 7 h. (c) Plot of the absorbance at 409 nm due to 4-NTP *versus* time. (d) PNIPAM-AuNPs and (e) NIPAM-AuNPs ($[Au^0] = 1.077 \times 10^{-4}$ M) under an LED reactor. (f) Plot of the absorbance at 409 nm due to 4-NTP *versus* time.

of 4-NTP by NIPAM-AuNPs in the dark was also attempted with similar concentrations (Fig. S15). No decrease in the absorbance is observed. To test their recyclability, the PNIPAM-AuNPs were reused in a second experiment to photodegrade 4-NTP under solar lamp illumination (Fig. S16). As observed, the nanoparticles show efficient catalytic activity and remain stable throughout the photoreduction process, confirming their reusability.

The photocatalytic activity of the NPs was also tested for the reduction of 4-NP under similar conditions to those used for 4-NTP; however, no degradation was observed within 6 hours of illumination.

In order to avoid the temperature increase due to the solar lamp illumination, the plasmonic activity of the synthesised AuNPs in the reduction of 4-NTP was investigated under LED illumination (Fig. 9). Both PNIPAM-AuNP and NIPAM-AuNP solutions with 4-NTP remained clear under LED illumination, indicating only a minor temperature increase (below the LCST of PNIPAM). However, the gradual decrease in the 4-NTP absorption peak (Fig. 9d and e) indicates the degradation of 4-NTP due to the plasmonic effects of the AuNPs activated by visible light. The temporal evolution of the absorbance at 409 nm due to 4-NTP is shown in Fig. 9f. The absorbance decay appears quasi-linear over time for NIPAM-AuNPs, exhibiting kinetics similar as those observed under solar lamp illumination.

Discussion on the (photo-)catalytic properties. The radiolytically synthesised PNIPAM-AuNPs and NIPAM-AuNPs exhibit efficient catalytic activity for the two model reactions tested: reduction of $[Fe(CN)_6]^{3-}$ by TEOA and reduction of 4-NP by $NaBH_4$. These results indicate that the AuNP surface remains accessible despite the presence of NIPAM oligomers or polymers, in agreement with previous results reported for chemically synthesised PNIPAM-AuNPs.[24,27,70] However, in the case of the ferrocyanate reduction, we have found that NIPAM oligomers or PNIPAM can protect small AuNPs (with an average diameter of 3.5 and 5.4 nm for NIPAM-AuNPs and PNIPAM-AuNPs, respectively) from degradation. Indeed, recently, Garai *et al.*[67] reported that AuNPs capped with polyvinylpyrrolidone (PVP) with diameters of 2 and 5 nm are dissolved during the reduction of $[Fe(CN)_6]^{3-}$ by TEOA, in contrast to those with a diameter of 13 nm, which remain essentially unchanged. Dissolution was not observed by Carregal-Romero *et al.*,[45] who used AuNPs with an average diameter of 60 nm. The dissolution is explained by the fact that the oxidation of gold also contributes to the reduction of $[Fe(CN)_6]^{3-}$, the oxidised gold being complexed by cyanide ions (CN^-) to form stable $Au(CN)_2^-$ in solution.[57,67] Sarhid *et al.* showed from XPS measurements that ligation of CN^- took place on the AuNPs' surface.[57] In our experiments with TEOA, after a small change upon the addition of $[Fe(CN)_6]^{3-}$ into the AuNPs' solution, the LSPR band remains unchanged during the reduction reaction performed in the dark, indicating that oxidation of gold does not occur. Nevertheless, under light illumination, a slight decrease is observed, suggesting that oxidation may occur associated with the transfer of generated hot electrons, but this oxidation does not increase the reaction rate of $[Fe(CN)_6]^{3-}$ reduction, in contrast to previous reports.[57,67]

Considering the reduction of 4-NP, an induction time is observed before the reaction occurs, following pseudo-first-order kinetics, as already reported in other studies.[47,69,71] This induction time, of the order of a few minutes, was attributed to a slow surface restructuring related to the presence of 4-NP.

Several mechanisms have also been proposed, and the role of $NaBH_4$ in AuNP-catalysed 4-NP reduction was previously studied.[72] Our results are in favour of the Langmuir–Hinshelwood model as described by Wunder *et al.*:[71] (i) BH_4^- ions react with the AuNPs surface and transfer a hydrogen to form a metal hydride, (ii) concomitantly, 4-NP molecules adsorb onto the surface, then, (iii) the reduction reaction takes place on the surface between adsorbed species to form 4-AP. Indeed, the reaction has been observed for 4-NP but not for 4-NTP, which can be attributed to the difference in the orientation of the pollutant molecules on the surface of the NPs, as evidenced by Cui *et al.*[11,14] They reported the complete reduction of 4-NP by $NaBH_4$ in the presence of gold nanostars (AuNS), but the absence of reaction for 4-NTP. They used surface-enhanced Raman scattering to monitor the interaction of the pollutants with the AuNS surface and found that 4-NP was absorbed *via* the nitro group, while 4-NTP was bound *via* the thiol group.[14] So, the direct contact of the nitro group with the AuNP surface is necessary for the catalysis. Regarding the apparent first-order rate constants, comparisons with other studies are difficult because there are several differences. For instance, Du *et al.*[27] observed a significantly faster catalytic reduction of 4-NP (within approximately 4 minutes) using chemically synthesised PNIPAM-AuNPs. The difference in the catalytic rate compared to the PNIPAM-AuNPs reported in this study can be attributed to differences in (i) nanoparticle size: while PNIPAM-AuNPs synthesised by Du *et al.*[27] were $\sim$2.3 nm in diameter, those in this study are $\sim$5.4 nm; (ii) surface accessibility and available sites: in the chemically synthesised PNIPAM-AuNPs, there is no radical-induced crosslinking of PNIPAM during synthesis.

The plasmonic photocatalytic properties of the synthesised AuNPs have also been tested in the absence of any reducing species or sacrificial electron donor for the same reduction reactions. The plasmonic reduction of $[Fe(CN)_6]^{3-}$ without TEOA occurs at the expense of the AuNPs. This indicates that hot electrons generated upon plasmon excitation are able to reduce $[Fe(CN)_6]^{3-}$, while the accompanying holes oxidise the nanoparticles. Similar results have already been reported by Garai *et al.*,[67] who explained the dissolution by the complexation of the oxidised gold atoms by cyanide ions (CN^-) to form stable $Au(CN)_2^-$ in solution.

For the photoreduction of nitroarenes, the reaction is observed for 4-NTP but not for 4-NP, indicating that the way the molecules are adsorbed on the surface plays a role, as discussed for the catalysis. However, in this case, adsorption by the thiol group appears favourable. In the absence of BH_4^-, there is no hydrogen present on the surface to reduce the nitro group into an amino group, which may explain why 4-NP does not undergo photoreduction under these conditions. In the case of 4-NTP, the reduction reaction is known to proceed *via* two main mechanistic pathways (Fig. 10). The first is the direct reduction of 4-NTP to 4-ATP, accompanied by the formation of several intermediates, including dihydroxylaminothiophenol (DHATP), nitrosothiophenol (NSTP), and hydroxylaminothiophenol (HATP).[73,74] The second is the indirect pathway, which involves the condensation of intermediates such as DHATP and HATP to form dimercaptoazobenzene (DMAB), which is subsequently reduced to 4-ATP.[73,75] Nuclear magnetic resonance (NMR) spectroscopy and mass spectrometry (MS) were employed to analyse the photocatalytic products of 4-NTP; several products were detected, but no clear signature was obtained. It is also worth noting that while the plasmonic excitation of the AuNPs allows the degradation of 4-NTP, the AuNPs remain stable and are not oxidised as in the case of $[Fe(CN)_6]^{3-}$. Such results suggest that the holes produced by plasmon excitation are scavenged.

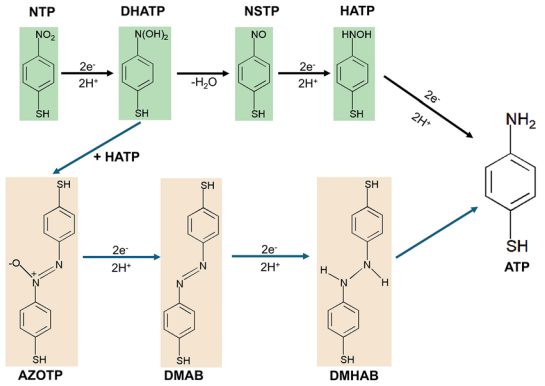

Fig. 10 Schematic representation of possible reaction pathways for the photocatalytic reduction of 4-nitrothiophenol to 4-aminothiophenol.[73,74]

Conclusion

In this study, gold nanoparticles stabilised by PNIPAM and NIPAM, PNIPAM-AuNPs and NIPAM-AuNPs, were synthesised in aqueous solutions using gamma radiation. The obtained AuNPs were spherical and quite homogeneous in size with average metallic diameters of 5.4 and 3.5 nm, respectively. In addition to the reduction of metallic ions, it was shown that irradiation initiated cross-linking of the thermosensitive PNIPAM, leading to a lowering of its LCST, and polymerisation of NIPAM monomers into small oligomers without thermosensitivity. It was found that the synthesised PNIPAM-AuNP and NIPAM-AuNP nanocomposites were very stable in solution for several months after irradiation.

The catalytic and photocatalytic activities of the synthesised PNIPAM-AuNPs and NIPAM-AuNPs were tested with two model reactions: the reduction of hexacyanoferrate, $[Fe(CN)_6]^{3-}$, and the reduction of the nitroarenes, *para*-nitrophenol (4-NP) and *para*-nitrothiophenol (4-NTP). The systems showed efficient catalytic activity towards the reduction of $[Fe(CN)_6]^{3-}$ and 4-NP, in the presence of TEOA or $NaBH_4$, respectively, used as electron donors or reducing agents. The systems also exhibited efficient photocatalytic properties by excitation of the plasmon resonance band of the AuNPs in the absence of an electron donor or reducing agent. However, in the case of $[Fe(CN)_6]^{3-}$, the reduction occurred at the expense of the AuNPs, which were oxidised and dissolved. In the case of 4-NTP, such degradation was not observed, and the AuNP systems remained stable

throughout the reaction. This result indicated that while the generated hot electrons reduced 4-NTP, the concomitantly produced holes were scavenged.

Our results also showed that, while the PNIPAM-AuNPs and NIPAM-AuNPs could catalyse the reduction of 4-NP by $NaBH_4$, no reaction took place with 4-NTP, and conversely, under plasmon excitation without a reducing agent, they could photodegrade 4-NTP but not 4-NP. These differences in reactivity might be explained by the different orientations of the adsorbed molecules on the metallic surface, through the nitro group for 4-NP and *via* the thiol group for 4-NTP.

Last but not least, the stabilisation of the AuNPs by the thermosensitive polymer appears highly efficient, as evidenced by the stability of the catalyst during the photocatalytic process and its reusability. Additionally, the thermosensitive polymer can offer more interesting catalytic properties to the AuNPs through its hydrophobic and hydrophilic properties, such as controlling the selectivity of the catalyst and hindering catalyst poisoning.[27]

Author contributions

Conceptualization: H. Remita, I. Lampre; formal analysis: T. Abdulyekeen, I. Lampre; investigation: T. Abdulyekeen, supervision: I. Lampre; validation: C. Sicard-Roselli, V. Huc, H. Remita; writing – original draft preparation: T. Abdulyekeen; writing – review & editing: T. Abdulyekeen, I. Lampre. All authors have read and agreed to the published version of the manuscript.

Conflicts of interest

There are no conflicts to declare.

Data availability

The data supporting this article have been included as part of the supplementary information (SI). Supplementary information: Fig. S1–S16. See DOI: https://doi.org/10.1039/d6nj00545d.

Acknowledgements

The authors acknowledge Mireille Benoit for her assistance in the chemistry laboratory and Alexandre Demarque for the access to the gamma irradiation facility at the Institut de Chimie Physique. The present work has also benefited from the Imagerie-Gif core facility supported by the French National Research Agency (ANR-24-INBS-0005 (BIOGEN); ANR-17-EUR-0007, EUR SPS-GSR) and from financial support from ITMO cancer of Aviesan and INCa with funds administered by Inserm.

References

1 N. Li, P. Zhao and D. Astruc, *Angew. Chem., Int. Ed.*, 2014, **53**, 1756–1789.
2 M. Chanana and L. M. Liz-Marzan, *Nanophotonics*, 2012, **1**, 199–220.
3 N. Nedyalkov, M. E. Koleva, R. Nikov, N. E. Stankova, E. Iordanova, G. Yankov, L. Aleksandrov and R. Iordanova, *Appl. Surf. Sci.*, 2019, **463**, 968–975.
4 L. M. Liz-Marzán, *Mater. Today*, 2004, **7**, 26–31.
5 R. D. Near, S. C. Hayden, R. E. Hunter Jr, D. Thackston and M. A. El-Sayed, *J. Phys. Chem. C*, 2013, **117**, 23950–23955.
6 S. Ali, X. Chen, W. Shi, G. Huang, L.-M. Yuan, L. Meng, S. Chen, X. Zhonghao and X. Chen, *Crit. Rev. Anal. Chem.*, 2023, **53**, 718–750.
7 J.-H. Lee, H.-Y. Cho, H. K. Choi, J.-Y. Lee and J.-W. Choi, *Int. J. Mol. Sci.*, 2018, **19**, 2021.
8 X. Cao, J. Feng, Q. Pan, B. Xiong, Y. He and E. S. Yeung, *Anal. Chem.*, 2017, **89**, 2692–2697.
9 P. Reineck, D. Brick, P. Mulvaney and U. Bach, *J. Phys. Chem. Lett.*, 2016, **7**, 4137–4141.
10 A. Woźniak, A. Malankowska, G. Nowaczyk, B. F. Grześkowiak, K. Tuśnio, R. Słomski, A. Zaleska-Medynska and S. Jurga, *J. Mater. Sci.: Mater. Med.*, 2017, **28**, 1–11.
11 Q. Cui, A. Yashchenok, L. Li, H. Möhwald and M. Bargheer, *Colloids Surf., A*, 2015, **470**, 108–113.
12 A. Taketoshi and M. Haruta, *Chem. Lett.*, 2014, **43**, 380–387.
13 P. Zhao, X. Feng, D. Huang, G. Yang and D. Astruc, *Coord. Chem. Rev.*, 2015, **287**, 114–136.
14 Q. Cui, B. Xia, S. Mitzscherling, A. Masic, L. Li, M. Bargheer and H. Moehwald, *Colloids Surf., A*, 2015, **465**, 20–25.
15 P. Bhol, M. Mohanty and P. S. Mohanty, *J. Mol. Liq.*, 2021, **325**, 115135.
16 S. T. Jones, Z. Walsh-Korb, S. J. Barrow, S. L. Henderson, J. Del Barrio and O. A. Scherman, *ACS Nano*, 2016, **10**, 3158–3165.
17 J. Hu, C. A. Brackemyer, H. Byun and J.-H. Kim, *J. Mater. Sci. Technol.*, 2014, **30**, 441–448.
18 M. G. Warner, S. M. Reed and J. E. Hutchison, *Chem. Mater.*, 2000, **12**, 3316–3320.
19 S. Johnson, S. Evans, S. Mahon and A. Ulman, *Supramol. Sci.*, 1997, **4**, 329–333.
20 A.-F. An, A.-H. Lu, Q. Sun, J. Wang and W.-C. Li, *Gold Bull.*, 2011, **44**, 217–222.
21 S. A. Siboro, D. S. Anugrah, K. Ramesh, Y. T. Jeong, Y.-S. Gal and K. T. Lim, *Mol. Cryst. Liq. Cryst.*, 2020, **704**, 24–34.
22 H. Kim, E. S. Daniels, V. L. Dimonie and A. Klein, *J. Polym. Sci., Part A: Polym. Chem.*, 2008, **46**, 912–925.
23 M. Ballauff, *Prog. Polym. Sci.*, 2007, **32**, 1135–1151.
24 S. S. Satapathy, P. Bhol, A. Chakkarambath, J. Mohanta, K. Samantaray, S. K. Bhat, S. K. Panda, P. S. Mohanty and S. Si, *App. Surf. Sci.*, 2017, **420**, 753–763.
25 L. Guo, J. Nie, B. Du, Z. Peng, B. Tesche and K. Kleinermanns, *J. Colloid Interface Sci.*, 2008, **319**, 175–181.
26 R. Li, C. Cheng, Z. Wang, X. Gu, C. Zhang, C. Wang, X. Liang and D. Hu, *Materials*, 2021, **14**, 443.
27 J.-T. Du, M. Qiao, Y. Pu, J.-X. Wang and J.-F. Chen, *Appl. Catal., A*, 2021, **624**, 118323.
28 P. Flemming, A. S. Münch, A. Fery and P. Uhlmann, *Beilstein J. Org. Chem.*, 2021, **17**, 2123–2163.

29 S. Z. Moghaddam and E. Thormann, *Curr. Opin. Colloid Interface Sci.*, 2020, **47**, 27–45.
30 H. G. Schild, *Prog. Polym. Sci.*, 1992, **17**, 163–249.
31 I. Idziak, D. Avoce, D. Lessard, D. Gravel and X. Zhu, *Macromolecules*, 1999, **32**, 1260–1263.
32 J.-F. Lutz and A. Hoth, *Macromolecules*, 2006, **39**, 893–896.
33 N. Nagaoka, A. Safrani, M. Yoshida, H. Omichi, H. Kubota and R. Katakai, *Macromolecules*, 1993, **26**, 7386–7388.
34 A. Halperin, M. Kröger and F. M. Winnik, *Angew. Chem., Int. Ed.*, 2015, **54**, 15342–15367.
35 E. H. N. Yong, K. Y. Tshai, A. B. Chai, S. S. Lim, I. Kong and E. H. Yap, *Intelligent Manufacturing and Mechatronics*, ed. R. A. Aziz, Z. Ismail, A. K. M. A. Iqbal, and I. Ahmed, Springer Nature, Singapore, 2024, pp. 327–337.
36 M. Karg, S. Jaber, T. Hellweg and P. Mulvaney, *Langmuir*, 2011, **27**, 820–827.
37 Z. Qian, K. N. Guye, D. J. Masiello and D. S. Ginger, *J. Phys. Chem. B*, 2017, **121**, 1092–1099.
38 M. Nguyen, N. Felidj and C. Mangeney, *Chem. Mater.*, 2016, **28**, 3564–3577.
39 C.-H. Zhu, Z.-B. Hai, C.-H. Cui, H.-H. Li, J.-F. Chen and S.-H. Yu, *Small*, 2012, **8**, 930–936.
40 D. J. Kim, S. M. Kang, B. Kong, W. J. Kim, H. J. Paik, H. Choi and I. S. Choi, *Macromol. Chem. Phys.*, 2005, **206**, 1941–1946.
41 H. Remita and I. Lampre, *Materials*, 2024, **17**, 364.
42 A. Abedini, A. A. A. Bakar, F. Larki, P. S. Menon, M. S. Islam and S. Shaari, *Nanoscale Res. Lett.*, 2016, **11**, 287.
43 W. Abidi and H. Remita, *Recent Pat. Eng.*, 2010, **4**, 170–188.
44 W. Abidi, P. Selvakannan, Y. Guillet, I. Lampre, P. Beaunier, B. Pansu, B. Palpant and H. Remita, *J. Phys. Chem. C*, 2010, **114**, 14794–14803.
45 S. Carregal-Romero, J. Perez-Juste, P. Hervés, L. M. Liz-Marzan and P. Mulvaney, *Langmuir*, 2010, **26**, 1271–1277.
46 C.-W. Yen and M. A. El-Sayed, *J. Phys. Chem. C*, 2009, **113**, 19585–19590.
47 T. Aditya, A. Pal and T. Pal, *Chem. Commun.*, 2015, **51**, 9410–9431.
48 M. Abdollahi and A. Mohammadirad, in *Encyclopedia of Toxicology*, ed. P. Wexler, 3rd edn, Academic Press, Oxford, 2014, pp. 575–577.
49 P. De Maria, A. Fini and F. M. Hall, *J. Chem. Soc., Perkin Trans. 2*, 1973, 1969–1971.
50 J. Zheng, *Microsc. Microanal.*, 2014, **20**, 1236–1237.
51 S.-i Yusa, K. Fukuda, T. Yamamoto, Y. Iwasaki, A. Watanabe, K. Akiyoshi and Y. Morishima, *Langmuir*, 2007, **23**, 12842–12848.
52 K. Kusolkamabot, P. Sae-ung, N. Niamnont, K. Wongravee, M. Sukwattanasinitt and V. P. Hoven, *Langmuir*, 2013, **29**, 12317–12327.
53 A. O. Govorov and H. H. Richardson, *Nano Today*, 2007, **2**, 30–38.
54 S. Sakane, T. Anji, I. Yamagishi, I. Kohara and H. Tanaka, *Chem. Lett.*, 2023, **52**, 582–585.
55 P. K. Jain, *J. Phys. Chem. C*, 2019, **123**, 24347–24351.
56 S. Ju, B. Palpant and Y. Chalopin, *J. Phys. Chem. C*, 2017, **121**, 13474–13480.
57 I. Sarhid, I. Lampre, D. Dragoe, P. Beaunier, B. Palpant and H. Remita, *Materials*, 2019, **12**, 3012.
58 A. Acharya, H. Mohan and S. Sabharwal, *J. Radiat. Res.*, 2003, **44**, 335–343.
59 C. Ferradini and J.-P. Jay-Gerin, *Can. J. Chem.*, 1999, **77**, 1542–1575.
60 E. Gachard, H. Remita, J. Khatouri, B. Keita, L. Nadjo and A. Jacqueline Belloni, *New J. Chem.*, 1998, **22**, 1257–1265.
61 M. Kumar, A. Panda and S. Sabharwal, *Radiat. Phys. Chem.*, 2000, **59**, 287–293.
62 M. K. Chumakov, L. Shahamat, A. Weaver, J. LeBlanc, M. Chaychian, J. Silverman, K. B. Richter, D. Weiss and M. Al-Sheikhly, *Radiat. Phys. Chem.*, 2011, **80**, 182–189.
63 A. S. Ghosh-Mazumdar and E. J. Hart, in *Radiation Chemistry*, ed. E. J. Hart, 1968, vol. 81, pp. 193–209.
64 G. R. Dey, *Radiat. Phys. Chem.*, 2014, **102**, 44–48.
65 G. R. Dey, A. K. El Omar, J. A. Jacob, M. Mostafavi and J. Belloni, *J. Phys. Chem. A*, 2011, **115**, 383–391.
66 A. Panda, S. B. Manohar, S. Sabharwal, Y. K. Bhardwaj and A. B. Majali, *Radiat. Phys. Chem.*, 2000, **58**, 101–110.
67 M. Garai, S. Diethör, F. Mayr, M. C. Scharber, N. S. Sariciftci and T. A. Klar, *J. Phys. Chem. C*, 2025, **129**, 6322–6331.
68 S. Kanimozhi and M. Kanthimathi, in *Nanoparticles in Green Organic Synthesis*, ed. S. Bhunia, B. Kumar, P. Singh, R. Oraon and K.-H. Kim, Elsevier, 2023, pp. 453–465.
69 P. Pongsanon, A. Kawamura, H. Kawasaki and T. Miyata, *Gels*, 2024, **10**, 357.
70 S. Carregal-Romero, N. J. Buurma, J. Pérez-Juste, L. M. Liz-Marzán and P. Hervés, *Chem. Mater.*, 2010, **22**, 3051–3059.
71 S. Wunder, F. Polzer, Y. Lu, Y. Mei and M. Ballauff, *J. Phys. Chem. C*, 2010, **114**, 8814–8820.
72 C. Deraedt, L. Salmon, S. Gatard, R. Ciganda, R. Hernandez, J. Ruiz and D. Astruc, *Chem. Commun.*, 2014, **50**, 14194–14196.
73 H.-K. Choi, W.-H. Park, C.-G. Park, H.-H. Shin, K. S. Lee and Z. H. Kim, *J. Am. Chem. Soc.*, 2016, **138**, 4673–4684.
74 W. Koopman, R. M. Sarhan, F. Stete, C. N. Schmitt and M. Bargheer, *Nanoscale*, 2020, **12**, 24411–24418.
75 B. Zhou, W. Ou, J. Shen, C. Zhao, J. Zhong, P. Du, H. Bian, P. Li, L. Yang and J. Lu, *ACS Catal.*, 2021, **11**, 14898–14905.